J Comp Physiol A (1997) 181: 532–544

ORIGINAL PAPER

M. E. Nelson · Z. Xu · J. R. Payne

Characterization and modeling of P-type electrosensory afferent responses to amplitude modulations in a wave-type electric fish

Accepted: 14 June 1997

Abstract The first stage of information processing in the electrosensory system involves the encoding of local changes in transdermal potential into trains of action potentials in primary electrosensory afferent nerve fibers. To develop a quantitative model of this encoding process for P-type (probability-coding) afferent fibers in the weakly electric fish *Apteronotus leptorhynchus*, we recorded single unit activity from electrosensory afferent axons in the posterior branch of the anterior lateral line nerve and analyzed responses to electronically generated sinusoidal amplitude modulations of the local transdermal potential. Over a range of AM frequencies from 0.1 to 200 Hz, the modulation transfer function of P-type afferents is high-pass in character, with a gain that increases monotonically up to AM frequencies of 100 Hz where it begins to roll off, and a phase advance with a range of 15–60 degrees. Based on quantitative analysis of the observed gain and phase characteristics, we present a computationally efficient model of P-type afferent response dynamics which accurately characterizes changes in afferent firing rate in response to amplitude modulations of the fish's own electric organ discharge over a wide range of AM frequencies relevant to active electrolocation.

Key words Computer simulation · Electrolocation
Electroreception · Neural model · Sensory coding

Abbreviations *AM* amplitude modulation · *DOF* degrees-of-freedom · EOD electric organ discharge · ISI interspike interval · pALLN posterior branch of anterior lateral line nerve · RMS root mean square

M.E. Nelson (✉) · Z. Xu · J.R. Payne
Department of Molecular and Integrative Physiology, and
The Beckman Institute for Advanced Science and Technology,
University of Illinois at Urbana-Champaign,
405 N. Mathews Ave., Urbana, IL 61801, USA
Tel.: + 1-217 244-1371; Fax: + 1-217 244-5180
e-mail: m-nelson@uiuc.edu

Introduction

The first stage of information processing in the electrosensory system of weakly electric fish involves the encoding of changes in transdermal potential experienced by electroreceptor organs in the skin into changes in spike activity on primary electrosensory afferent nerve fibers (Bastian 1986a, 1995; Zakon 1986). During active electrolocation, nearby objects with an impedance different from the surrounding water perturb the transdermal potential established by the fish's own electric organ discharge (EOD). In the gymnotiform species *Apteronotus leptorhynchus* (brown ghost knife fish), which has a continuous quasi-sinusoidal wave-type EOD waveform, these object-induced perturbations give rise to amplitude modulations (AMs) of the EOD carrier signal. Thus studying the encoding of electrolocation signals by electrosensory afferents in this species and other wave-type electric fish involves determining how afferent spike activity is influenced by AM stimuli.

Changes in transdermal potential are detected by tuberous electroreceptor organs that are specialized for detecting modulations of signals near the carrier frequency of the EOD (Zakon 1986). In gymnotiform wave species, tuberous afferents can be classified into two functional categories: P units and T units (Scheich et al. 1973). Under natural conditions, T units (time coders) fire regularly with one spike per EOD cycle, independent of the stimulus intensity, and thus convey timing information. P units (probability coders) fire irregularly with a per-cycle firing probability that depends on stimulus intensity, and thus convey amplitude information. In this paper we develop a quantitative model of the AM response characteristics of P-type afferent nerve fibers in *A. leptorhynchus* based on the analysis of single unit activity recorded from axons in the posterior branch of the anterior lateral line nerve (pALLN), which innervates trunk electroreceptor organs.

Previous studies of P units in gymnotiform electric fish have revealed a great deal about their AM response characteristics, yet some important issues remain to be resolved. Earlier studies demonstrated that P units exhibit high-pass filtering characteristics in response to step and sinusoidal AM stimuli; however, there was a large variation in the reported time constants. Studies using AM steps reported adaptation time-constants ranging from 0.2 to 3.4 s (Hagiwara et al. 1965; Scheich et al. 1973; Hopkins 1976; Shumway and Maler 1989). Studies using AM sinusoids showed that the gain is monotonically increasing up to AM frequencies of at least 64 Hz where it begins to roll off (Bastian 1981): a high-pass filter with a corner frequency near 64 Hz should have a corresponding time-constant in the range of 2.5 ms ($1/2\pi f$). A recent analysis using stochastically generated AM stimuli obtained linear filters for optimal stimulus reconstruction that were consistent with high-pass response characteristics (Wessel et al. 1996). Thus, previous studies were in agreement regarding the high-pass nature of the response, but estimates of the dominant filter time-constants ranged from milliseconds to seconds.

We have recently presented new experimental results suggesting that the large variance in previously reported time-constants may be related to our observation that the adaptation to AM step stimuli in P-type afferents actually follows a time-course that is better described as logarithmic rather than exponential (Xu et al. 1996). The distributed dynamics that are likely to underlie the logarithmic adaptation time-course can give rise to apparent time-constants ranging from milliseconds to tens of seconds, depending on how the data are collected and analyzed. In this paper we combine insights from the study of Xu et al. (1996) which focused on P unit responses to AM steps, with new experimental results on responses to AM sinusoids. Based on these findings, we construct a model of P-type afferent response dynamics which accurately characterizes responses over a wide range of stimuli relevant to active electrolocation.

Materials and methods

A total of eight adult (12–17 cm long) weakly electric fish of the species *Apteronotus leptorhynchus* (brown ghost knife fish) obtained from local suppliers were used in this study. Fish were housed in laboratory aquaria and maintained on a 12:12 h light-dark cycle. Water conditions in the holding tanks were maintained at a temperature of 27–28 °C, pH of 6.5–6.9, and conductivity of 200–300 $\mu S\ cm^{-1}$. Experiments were carried out in the middle of a rectangular Plexiglas tank (41 × 41 × 15 cm). Water conditions in the experimental tanks were adjusted to match the temperature, pH and conductivity of the home tanks.

Surgical procedure

Fish were lightly anesthetized by immersion in 100 ppm tricaine methanesulfonate (MS-222, Sigma) for 2 min, then immobilized with an intramuscular injection of 3 µl of 10% gallamine triethiodide (Flaxedil, Sigma), and subsequently respirated with a constant flow of fresh aerated water provided through a mouth tube. The EOD from the neurogenic electric organ remained intact following the Flaxedil injection. Fish were gently held with their right side against a foam pad on a Plexiglas stand in the middle of the experimental tank with the dorsal surface of the head slightly higher than the rest of the body, such that the site of surgical exposure was just above the water level and most of the electroreceptors on the trunk of the fish were submerged. The posterior branch of the left anterior lateral line nerve, which innervates trunk electroreceptors, was exposed approximately 1 mm rostral to the insertion of the pectoral fin, immediately dorsal to the lateral line. Lidocaine hydrochloride (2%) was applied locally to the skin prior to nerve exposure. The exposed nerve was periodically bathed in Ringer's solution (Bastian 1974) throughout the experiment. All surgical procedures were reviewed and approved by the Laboratory Animal Care and Advisory Committee at the University of Illinois at Urbana-Champaign.

Nerve recording

Action potentials from individual pALLN afferents were recorded with sharp glass micropipettes (impedance 10–30 MΩ) filled with 3 $mol\ l^{-1}$ KCl solution. The recording electrode was positioned in the intact nerve using a piezoelectric microdrive (Burleigh 7010). Nerve activity was recorded differentially with a unity-gain DC preamplifier (A-M Systems 1600), amplified by an AC amplifier (A-M Systems 1700) with a gain of 1000, and bandpass filtered between 10 Hz and 5 kHz (40 dB/decade rolloff). A reference signal for the differential recording was provided by a fine silver wire electrode positioned in the exposure site near the nerve, so as to minimize the artifact from the fish's EOD.

The pALLN carries afferent fibers from both ampullary and tuberous electroreceptors; only P-type tuberous afferents were recorded in these experiments. Tuberous afferents were identified by applying a 5-Hz sinusoidal AM "search stimulus" to the experimental bath (see below) to preferentially excite tuberous receptors. Ampullary receptors did not respond to this AM search stimulus. A few T-type tuberous afferents which are easily identified by their regular firing pattern at the EOD frequency were encountered over the course of these experiments, but were not studied. The vast majority of tuberous afferents in the pALLN are P-type, and can be readily identified by an irregular baseline firing pattern which can be modulated by the search stimulus. No attempt was made in this study to determine the precise location of the electroreceptor organ corresponding to each P-type afferent fiber. A total of 109 P-type afferents in eight fish were analyzed in this study.

Stimulation

Stimuli consisted of externally imposed AMs of the quasi-sinusoidal transdermal potential established by the fish's own EOD. The fish's EOD signal was monitored with a pair of carbon electrodes placed near the head and tail of the fish. AM waveform envelopes were generated with a programmable arbitrary function generator (Wavetek 95), scaled to the desired intensity with a programmable attenuator (Weinschell 3210), multiplied with the EOD carrier signal using an analog multiplier (Tucker-Davis MT3) and delivered to the experimental tank through an optical stimulus isolator (A-M Systems 2200) via two 31-cm-long, 1.3-cm-diameter carbon rods. The rods were placed on opposite sides of the fish, parallel to the rostral-caudal axis, 17 cm from the midline. In this configuration, current flow due to external stimulation is parallel to medial-lateral axis of the body (transverse stimulus geometry). For some receptor locations, particularly near the tail region of the fish, the AM stimulus also introduced minor phase modulations (typically $< 10°$). These phase modulations do not affect the results of our studies, since the firing probability of P units is insensitive to smooth phase modulations, such as those induced by our stimulus (Heiligenberg and Partridge 1981).

Calibration

The AM stimulus intensity was calibrated with respect to the transdermal potential change measured between an intramuscular reference electrode placed in the fish's back, and a recording electrode outside the skin on the lateral trunk of the fish. Baseline (unstimulated) transdermal potentials had a root mean square (RMS) value ranging from 0.6 to 1.8 mV RMS. A zero dB stimulus was defined as one that produced a 1 mV RMS increase in transdermal potential. Stimulus intensities used in these studies ranged from −40 dB (10 µV RMS) to 0 dB (1 mV RMS). When characterizing response linearity, stimulus intensities between −40 dB and 0 dB in 5-dB increments were used. When characterizing the frequency dependence of response gain and phase, the stimulus intensity was adjusted so as not to drive the unit into firing rate saturation or rectification; typical intensities were −30 to −10 dB.

Data collection and analysis

Nerve activity, transdermal potential and timing signals were digitally sampled at 17 kHz with custom data acquisition software running on a Sun workstation (SPARCstation 2) equipped with a multifunction data acquisition card (Analyx Systems ADDA1418-166) and stored on magnetic disk for further processing. Spike events in the nerve recording were identified by a threshold criterion and time-stamped with a resolution of 60 µs. All data analysis procedures were carried out on Sun workstations using both custom software and the commercially available software package MATLAB (The MathWorks).

Responses to sinusoidal AM stimuli were analyzed by constructing cycle histograms of afferent spike times relative to the stimulus cycle with 20 bins per cycle. The total stimulus duration at each frequency was 10 s, independent of stimulus frequency. Before constructing the cycle histograms, all spike times were shifted by −2.5 ms to account for the mean response latency due to synaptic and axonal transmission delays as measured from responses to AM step stimuli. A fixed time shift was used because the mean latency was more reliable than the estimates obtained for individual afferents. The standard deviation of the measured latency distribution was about 0.6 ms, which is reflected in the error bars assigned to our phase estimates. The spike count in each bin was divided by the product of the bin width and the total number of stimulus cycles, such that the ordinate of the cycle histogram corresponded to afferent firing rate in spikes per second. A single cycle of a sinusoidal waveform was fit to the observed spike rate modulation $r(x) = A\sin(2\pi x + \phi) + c$, where x is the cycle fraction ($0 \le x \le 1$), A is the amplitude, ϕ is the phase and c is the offset. Fits were performed by minimizing the χ^2 between the predicted and observed rate change using a constrained optimization routine provided in the MATLAB Optimization Toolbox. The gain of the response at each AM stimulus frequency was computed as the ratio of the best-fit amplitude parameter for the sinusoidal spike rate modulation to the amplitude of the AM stimulus waveform. Thus, gain is expressed in units of spikes per second change in afferent firing rate per mV RMS change in transdermal potential. The phase of the response at each frequency was given by the best-fit phase parameter for the sinusoidal spike rate modulation.

Parameterizing the frequency response characteristics

The frequency dependence of the gain and phase is parameterized by a second-order linear systems model with a transfer function $H(s)$, given by:

$$H(s) = \frac{G_a s}{s + 1/\tau_a} + \frac{G_b s}{s + 1/\tau_b} + G_c \qquad (1)$$

where s is the complex frequency ($s = i\omega$), $G_{a\text{–}c}$ are gain terms with units of spikes s^{-1} mV^{-1}, τ_a and τ_b are time-constants with units of seconds. This model is equivalent to two first-order high-pass filters in parallel with a constant gain element. At a particular AM frequency $f = \omega/2\pi$, the overall gain is given by $G(f) = |H(s)|$ and the phase of the response is $\phi(f) = \tan^{-1}(\operatorname{Im} H(s)/\operatorname{Re} H(s))$. When comparing responses among different units, we will use a normalized form of the transfer function $H_{\mathrm{norm}}(s)$ which is rescaled to have a normalized gain $G_{\mathrm{norm}}(f)$ of unity at an AM frequency of 1 Hz:

$$H_{\mathrm{norm}}(s) = \frac{H(s)}{G_{1\,\mathrm{Hz}}} = \frac{g_a s}{s + 1/\tau_a} + \frac{g_b s}{s + 1/\tau_b} + g_c \qquad (2)$$

where $G_{1\,\mathrm{Hz}} = G(f = 1) = H(i2\pi)$ is the overall gain at 1 Hz, and g_a, g_b, and g_c are dimensionless terms corresponding to $G_a/G_{1\,\mathrm{Hz}}$, $G_b/G_{1\,\mathrm{Hz}}$ and $G_c/G_{1\,\mathrm{Hz}}$. Best-fit parameter values for the gain and time constant parameters in Eqs. 1 and 2 were determined by fitting these functional forms to the observed gain and phase data using a χ^2 minimization procedure.

Computer simulations of afferent responses

Computer simulations of P-type afferent responses were implemented in MATLAB on a Sun SPARCstation 20/712 workstation. Numerical integration was carried out using a fixed integration time-step corresponding to one EOD period. Dynamic state variables in the model were updated using a numerical integration routine (LSIM) provided in the MATLAB Control System Toolbox that computes the exact solution to the update equations for a linear system at each time step assuming the inputs to the system remain constant during each step. Simulated data sets were generated using stimulus protocols that mimic those used in our experimental studies. Spike times and stimulus-related timing signals from the simulation were stored on magnetic disk and subsequently analyzed using the same data analysis techniques as described above for our analysis of experimental data.

Angular dependence

In one experiment designed to study the effects of stimulus orientation, the fish was suspended in the center of a 24-cm-diameter cylindrical tank in a vertical position by means of sutures through the upper and lower lips. Two stimulus rods mounted on a rotating platform were placed vertically on opposite sides of the fish parallel to the rostral-caudal axis 8.5 cm from the midline. By rotating the platform holding the stimulus rods, the stimulus orientation could be changed continuously from the normal transverse geometry (0 degrees), in which externally imposed current flow is parallel to the medial-lateral axis of the body, to stimulus angles of ±90° in which externally imposed current flow is parallel to the dorsal-ventral axis of the body.

Results

Baseline activity

Baseline firing rates of P-type afferents in the presence of the EOD but without any externally imposed stimulus ranged from 108 to 599 spikes s^{-1} with a mean of 321 ± 110 spikes s^{-1} ($n = 109$ units). The EOD frequency of individual fish was constant and ranged from 730 to 1002 Hz ($n = 8$ fish). P-type afferents fire at most one spike per EOD cycle; under baseline conditions the firing probability per EOD cycle ranged from 0.11 to 0.61 (Fig. 1A) with a mean of 0.36 ± 0.12 ($n = 109$). Spike times are loosely phase-locked to the EOD cycle, giving rise to multimodal interspike interval (ISI) distributions with peaks occurring at integral multiples of the EOD period. Three representative baseline ISI distributions are shown in Fig. 1B–D. The distribution in Fig. 1B has a large number of single-cycle intervals and a long tail extending out past 10 EOD periods with a mean ISI of

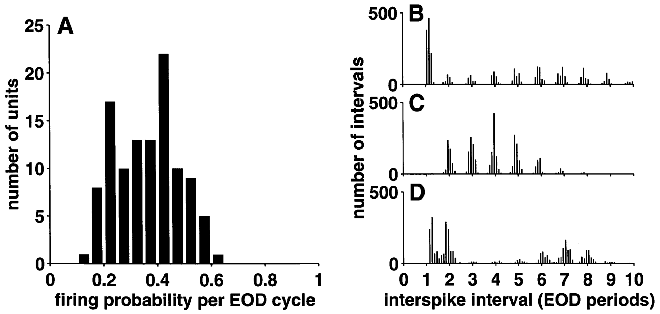

Fig. 1A–D Baseline firing characteristics of P-type afferents. **A** Mean baseline firing probability per EOD cycle for the 109 units in the sample. **B–D** Representative interspike interval (ISI) histograms for three individual units, all of which have similar baseline firing rates. The unit shown in **B** has an irregular firing pattern, while **C** is more regular and **D** is bursty

4.2 EOD periods. The distribution in Fig. 1C has a similar mean (3.9 EOD periods), but the intervals are more tightly clustered between 2 and 6 EOD periods. The distribution in Fig. 1D also has a similar mean (4.2 EOD periods), but has a characteristic "bursty" signature with a large number of one- and two-cycle intervals arising from spike doublets and triplets, separated by gaps of 6–8 EOD cycles. The ISI distributions observed in this study do not appear to fall into distinct categories, but rather appear to be drawn from a continuum of ISI characteristics, ranging from irregular (Fig. 1B, D) to regular (Fig. 1C) and from non-bursty (Fig. 1B, C) to bursty (Fig. 1D). A quantitative approach for characterizing the degree of burstiness in P-type afferents has been described in an earlier study (Xu et al. 1996).

Responses to single-frequency AM sinusoids

In response to single-frequency sinusoidal AM stimulation, P-type afferents typically showed a smooth sinusoidal modulation in firing rate around their baseline rate. The gain and phase of the response to sinusoidal AM stimulation was measured at 11 different AM frequencies ranging from 0.1 to 200 Hz in 99 units. Figure 2A shows cycle histograms for one representative P unit at the 11 AM frequencies tested. Figures 2B and 2C show the best-fit values of gain and phase at each AM frequency as determined by fitting a single cycle of a sine function with variable amplitude and phase to each cycle histogram (solid lines in Fig. 2A). The large error bars for the high-frequency phase points (Fig. 2C) are associated with a variability of about 0.6 ms in our measurements of the response latency of the system. This timing uncertainty translates into large phase uncertainties at high frequencies (e.g., 43° at 200 Hz), but is negligible at low frequencies (e.g., 0.2° at 1 Hz). The variability in response latency is due to several factors, including differences in axonal transmission delays, stimulus intensity, and afferent sensitivity. Axonal delays associated with receptor location on the body are

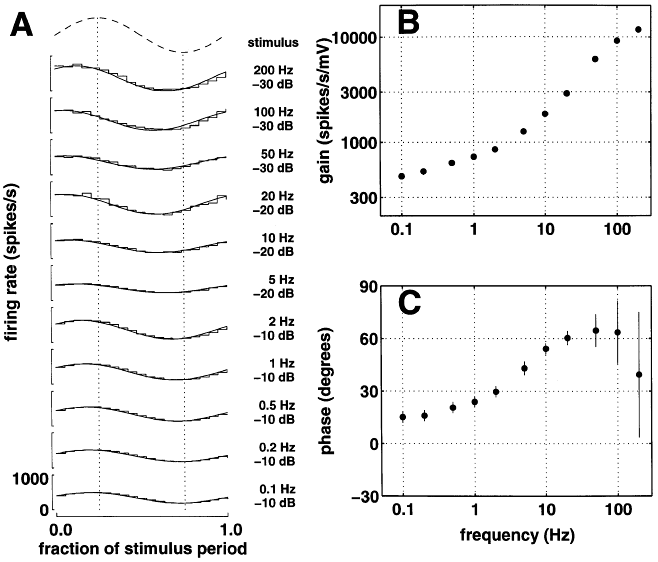

Fig. 2A–C Response of a single P unit to transverse sinusoidal AM stimulation at frequencies between 0.1 and 200 Hz. **A** Cycle histograms showing the modulation in afferent firing rate with respect to the stimulus cycle for the 11 AM frequencies tested. Histogram values are plotted in a stairstep fashion. The *continuous solid lines* are best-fit single cycle sinusoids. *Vertical dotted lines* indicate the times of the maximum and minimum of the AM stimulus waveform. **B** Gain versus AM frequency for this unit, as determined from the sinusoidal fits in A. Error bars are smaller than the plot symbols and therefore not visible. **C** Phase versus AM frequency for this unit, as determined from the sinusoidal fits in **A**. Error bars reflect the combined uncertainty from the fit and an uncertainty associated with the absolute response latency which results in larger error bars for higher AM frequencies

known to be partially compensated by variations in axon diameter (Heiligenberg and Dye 1982).

The AM transfer function is high-pass in character with a gain that increases monotonically with increasing AM frequency and a phase that leads the stimulus (i.e., the peak of the response precedes the peak of the stimulus) by about 15–60°. This phase lead reflects the fact that the afferent system is sensitive to the slope as well as the magnitude of the stimulus. The gain and phase characteristics were strikingly similar in all 99 units tested. To compare gain curves across units we first divided the gain at each frequency by the gain at 1.0 Hz to compute a normalized gain (which is thus unity at 1 Hz). Figure 3 shows the mean normalized gain and mean phase of the response averaged over the population. The small variation in response characteristics across the population is particularly striking for AM frequencies below 20 Hz where the coefficient of variation (standard deviation/mean) for normalized gain was less than 5% and the standard deviation of the phase was less than 5°.

The solid curves in Fig. 3 are the gain and phase corresponding to the normalized transfer function in Eq. 2, with parameter values obtained from a minimum χ^2 fit to the population averaged response data. The best-fit parameter values were: $g_a = 11.3$, $g_b = 0.37$, $g_c = 0.63$, $\tau_a = 0.0029$ s, and $\tau_b = 0.318$ s. The χ^2 was 11.7 for 18 degrees of freedom (DOF), indicating a good

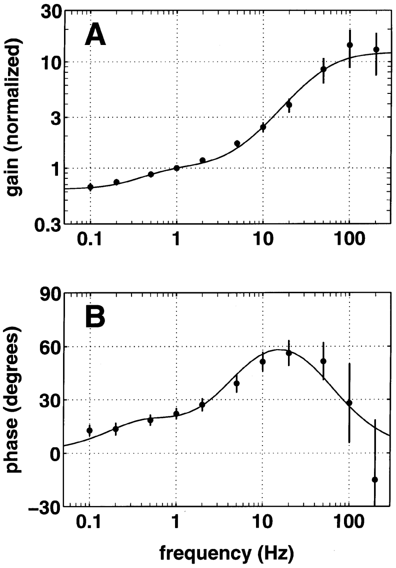

Fig. 3A, B Population-averaged P unit response characteristics. **A** Mean normalized gain versus AM frequency. **B** Mean phase versus AM frequency. Error bars represent the standard deviation of the population average at each frequency. The *continuous solid lines* show the gain and phase from a linear systems model of the form given in Eq. 2 with best-fit parameters: $g_a = 11.3$, $g_b = 0.37$, $g_c = 0.63$, $\tau_a = 0.0029$ s, and $\tau_b = 0.318$ s

fit to the data. Figure 4 illustrates the contributions of the three terms in Eq. 2 to the overall gain and phase of the response. For AM frequencies above about 20 Hz, the gain and phase are dominated by the contribution of the first term in Eq. 2, corresponding to a high-pass filter with a time-constant $\tau_a = 0.0029$ s (dashed line in Fig. 4). For AM frequencies below about 0.2 Hz, the response is dominated by the constant gain term g_c (dotted line in Fig. 4). For intermediate AM frequencies between about 0.2 and 20 Hz, all three terms make a significant contribution to the response.

The linear systems model in Eq. 2 was also used to fit the AM frequency response data from each of the 99 units individually. Figure 5 summarizes the best-fit parameter values obtained from fits to individual unit responses. The means and standard deviations for the best-fit parameter values were: $g_a = 14.1 \pm 7.7$, $g_b = 0.47 \pm 0.11$, $g_c = 0.67 \pm 0.06$, $\tau_a = 0.0026 \pm 0.0013$ s, and $\tau_b = 0.21 \pm 0.07$ s. The mean χ^2 per DOF was 1.39 ± 1.44, indicating that Eq. 2 provided a good fit to the individual unit responses; the distribution of χ^2 per DOF is shown in Fig. 5F. The parameter distributions in Fig. 5A–E appear to be predominantly unimodal and thus suggest that the afferents in this sample are drawn from a population with homogenous response dynamics, consistent with the small standard deviations in the population averaged gain and phase data shown earlier in Fig. 3.

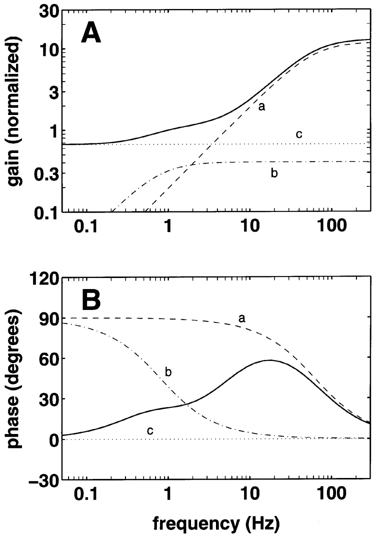

Fig. 4A, B Individual contributions of the high-pass filter and constant gain terms in Eq. 2 to the overall response shown in Fig. 3. **A** Normalized gain versus AM frequency. **B** Phase versus AM frequency. *Dashed line*: $H_a(s) = g_a s/(s + 1/\tau_a)$; *dash-dot*: $H_b(s) = g_b s/(s + 1/\tau_b)$ *dotted*: $H_c(s) = g_c$; *solid line*: $H_{norm}(s) = H_a(s) + H_b(s) + H_c(s)$. Note that the overall gain and phase cannot be computed by simply summing the component gains and phases, but at frequencies where the gain of one of the components $G_x(f)(= |H_x(s)|)$ is much larger than the other two, $G(f) \approx G_x(f)$ and $\phi(f) \approx \phi_x(f)$

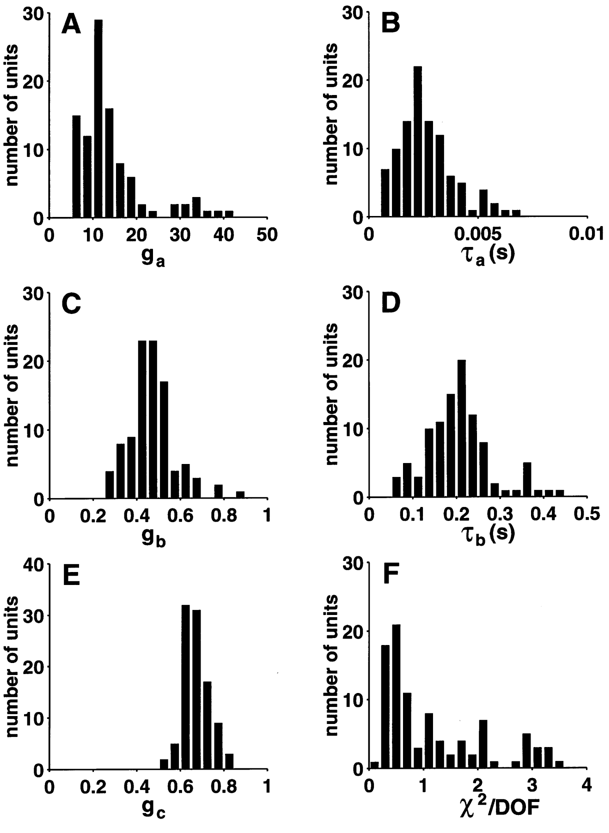

Fig. 5A–F Summary of results obtained from fits of the form in Eq. 2 to individual P unit frequency response profiles. **A–E** Distribution of best-fit values for g_a, τ_a, g_b, τ_b and g_c, respectively. **F** Distribution of the χ^2 per degrees-of-freedom (DOF), a measure of the goodness-of-fit

Estimating absolute response sensitivity

The sensitivity of tuberous afferents is inherently directional (Yager and Hopkins 1993), presumably as a result of the structural organization of the electroreceptor organ. To verify that the afferent response amplitudes we measured are indeed dependent on stimulus angle, a control experiment was carried out in which a fish was suspended vertically and the stimulus angle could be changed by rotating a pair of stimulus rods about the vertical axis. Figure 6 shows a typical response profile from one of the nine units recorded in this study, demonstrating an approximately sinusoidal dependence of the response amplitude on stimulus angle.

Except for the data shown in Fig. 6, all responses in this study were collected using a fixed transverse stimulus geometry (see Materials and methods). Therefore, the quantity we have measured is the "transverse" gain of the afferents, namely the sensitivity to transdermal potential modulations imposed in a transverse direction (lateral to medial) across the body of the fish. For the units in our sample the transverse gain at 1 Hz, $G_{1\,\mathrm{Hz}}$, ranged from 142 to 2045 spikes s^{-1} mV^{-1} with a mean of 626 ± 328 spikes s^{-1} mV^{-1} ($n = 99$), as shown in Fig. 7. The transverse gain is typically less than the maximum gain which would be observed at the optimal stimulus orientation.

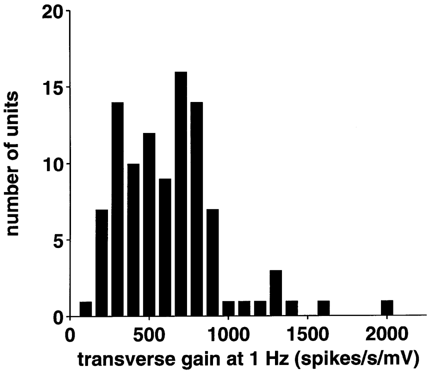

Fig. 7 Distribution of the transverse gain of P units at an AM frequency of 1 Hz. Transverse gain is a measure of the sensitivity of P units to stimuli delivered using the fixed transverse stimulus geometry described in the Materials and methods section. The transverse gain is typically less than the maximum gain that would be measured with an optimally oriented stimulus

Response linearity

The output dynamic range of P-type afferents is limited in that they exhibit both firing rate rectification (firing rates cannot be less than zero) and firing rate saturation (firing rates cannot exceed the EOD frequency); thus, strong AM stimuli can give rise to non-linear P unit responses. For weaker AM stimuli that do not drive the units into rectification or saturation, we found that afferent responses scaled almost linearly with stimulus amplitude. Figure 8A shows responses to a 1-Hz AM stimulus with intensities ranging from –40 dB to 0 dB; note the marked clipping of the response for the 0 dB stimulus. The solid curves in Fig. 8A are single cycle sinusoids fit to the non-clipped portion of the cycle histograms. The amplitudes of these best-fit sinusoids are plotted as a function of stimulus intensity in Fig. 8B, showing that the response scales almost linearly with stimulus amplitude. The solid line in Fig. 8B shows the best-fit to the stimulus-response data assuming perfect linearity (i.e., $y = Ax$, where y is the response amplitude and x is the stimulus intensity), while the dashed line in Fig. 8B shows the best-fit power law form ($y = Ax^{\mathrm{B}}$) which provides a slightly better fit to the data with $B = 0.89$. Response linearity was analyzed in this man-

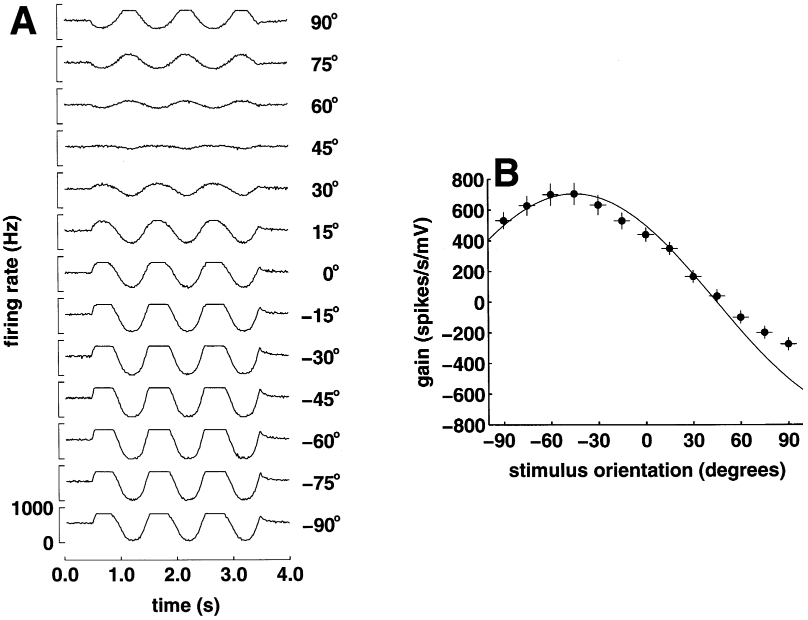

Fig. 6A, B Influence of stimulus orientation on apparent gain of P units. **A** Firing rate modulations in response to a 1-Hz AM sinusoidal stimulus applied at various stimulus angles; transverse stimulation corresponds to 0°. **B** Apparent gain as a function of stimulus angle. The *continuous solid curve* is a best-fit sinusoid. *Vertical error bars* represent uncertainties in gain; *horizontal error bars* represent uncertainties in the angular position relative to the receptor pore

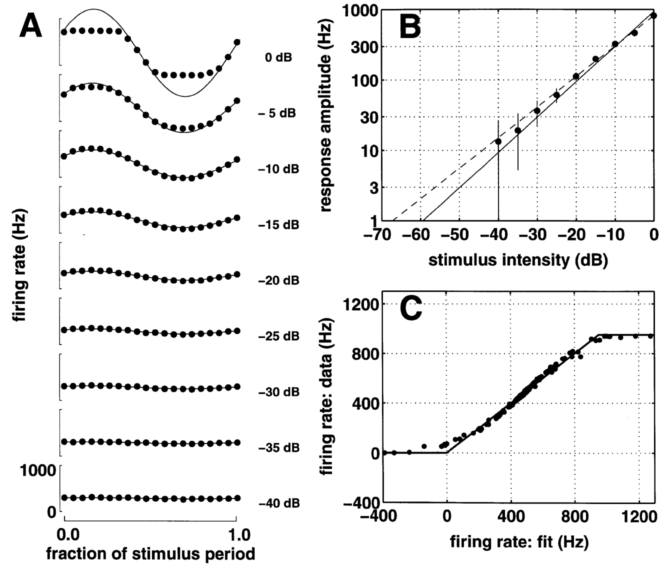

Fig. 8A–C Effects of stimulus intensity on P unit response amplitude. **A** Cycle histograms for a representative unit showing the modulation in afferent firing rate for a 1-Hz stimulus with intensities from −40 dB (10 μV RMS) to 0 dB (1 mV RMS). Histogram values are shown as data points; best-fit sinusoids are shown as *continuous solid lines*. **B** Response amplitude versus stimulus intensity for the unit shown in **A** (data points). The *solid line* is the best-fit linear response function ($y = 937x$); the *dashed line* is the best-fit power law function ($y = 829x^{0.89}$). **C** Comparison of actual response amplitude versus fit amplitude for all the cycle histogram data points in **A**. The *solid line* represents the clipping non-linearity (Eq. 5) associated with firing rate rectification and saturation

ner for 24 units in five fish and in all cases the power law form gave a slightly better fit to the data. The best-fit values for B ranged from 0.83 to 0.95 with a mean of 0.90 ± 0.04 ($n = 24$). Figure 8C illustrates the shape of the clipping non-linearity by comparing the firing rate predicted by the best-fit (unclipped) sinusoid to the actual measured firing rate for each data point in Fig. 8A.

Another test for response linearity involves comparing the response of a system to stimuli presented individually to the response when the stimuli are presented together. For a linear system, the response to a sum of input signals should be equal to the sum of the responses for each input alone. We tested the linearity of P-type afferents by comparing responses to single frequency AM sinusoids of 1, 10 and 100 Hz with responses to a combination of these three frequencies presented simultaneously. For each frequency component, we compared the gain and phase measured with all three frequencies combined (G_{combined}, ϕ_{combined}) relative to the gain and phase when each frequency was presented in isolation (G_{alone}, ϕ_{alone}). The mean fractional gain change $(G_{\mathrm{combined}}-G_{\mathrm{alone}})/G_{\mathrm{alone}}$ was 0.001 ± 0.02, 0.03 ± 0.05, and -0.14 ± 0.09 for 1, 10 and 100 Hz, respectively ($n = 10$). The mean phase change ($\phi_{\mathrm{combined}}-\phi_{\mathrm{alone}}$) was 1.2 ± 1.8°, 2.6 ± 1.5° and 34 ± 12° for 1, 10 and 100 Hz, respectively ($n = 10$). Thus, when all three frequencies were presented together there was no significant change in gain or phase for the 1 and 10 Hz components, while there was a modest 14% gain decrease and 34° phase advance for the 100-Hz component. This suggests that there are only minor nonlinearities associated with cross-frequency interactions in this AM frequency range.

An integrated model of P-type afferent response dynamics

We have incorporated the response characteristics illustrated in Figs. 1–8 into an integrated model of P-type afferent response dynamics. The model, illustrated in Fig. 9, consists of three key elements: (1) a linear systems model that captures the frequency dependence of the AM response characteristics, (2) a static non-linearity that models the effects of firing rate rectification and saturation, and (3) a stochastic spike generator that transforms continuous firing rates into trains of discrete spikes that are phase-locked to the EOD cycle. The model also incorporates the baseline firing rate and takes into account the latency in the response due to synaptic delays and axonal propagation delays. The linear systems portion of the model is based on Eq. 1 with parameter values determined from fits to gain and phase response data. The time-domain response of the linear model is given by the following pair of equations:

$$\begin{aligned} \dot{x} &= Ax + Bu \\ y &= Cx + Du \end{aligned} \tag{3}$$

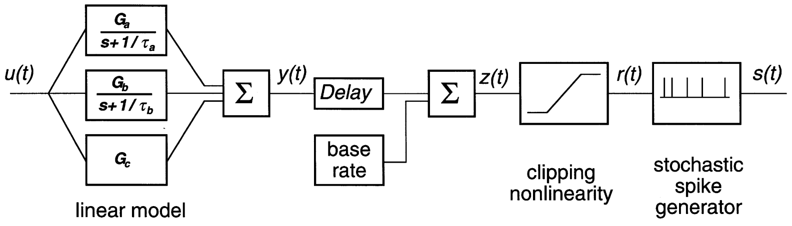

Fig. 9 Model of P-type electrosensory afferent response dynamics. The model input is the time-varying amplitude of the AM stimulus envelope $u(t)$. The stimulus is transformed by the linear model as described by Eq. 1, which consists of three elements in parallel: two first-order high-pass filters and a constant gain term. The output of the linear model is delayed to simulate the effects of synaptic and axonal propagation delays, a constant baseline firing rate is added, and the resulting signal is passed through a static non-linearity which incorporates the effects of firing rate rectification and saturation. The instantaneous firing rate $r(t)$ is then converted into a binary spike train $s(t)$ by a stochastic spike-generating element

where $u(t)$ is the time-varying envelope of the AM stimulus, $y(t)$ is the output and $x(t)$ is a vector of two internal state variables associated with the two high-pass filters shown in Fig. 9.

$$A = \begin{bmatrix} -1/\tau_\mathrm{a} & 0 \\ 0 & -1/\tau_\mathrm{b} \end{bmatrix} \quad B = \begin{bmatrix} G_\mathrm{a}/\tau_\mathrm{a} \\ G_\mathrm{b}/\tau_\mathrm{b} \end{bmatrix} \quad C = [-1\ -1]$$
$$D = (G_\mathrm{a} + G_\mathrm{b} + G_\mathrm{c}) \tag{4}$$

The output of the linear model $y(t)$ is delayed by an amount t_d, and a baseline firing rate r_base is added: $z(t) = y(t - t_\mathrm{d}) + r_\mathrm{base}$. The signal $z(t)$ is the input to a clipping non-linearity which incorporates the effects of firing rate rectification and saturation:

$$r(t) = \begin{cases} 0 & z(t) < 0 \\ z(t) & 0 \le z(t) \le f_\mathrm{EOD} \\ f_\mathrm{EOD} & z(t) > f_\mathrm{EOD} \end{cases} \tag{5}$$

where $r(t)$ is the output firing rate, and f_EOD is the EOD frequency.

A stochastic spike-generating element converts the output firing rate $r(t)$ into a binary spike train $s(t)$. In its simplest form, the spike-generating element computes the probability $p(t)$, of generating a spike on each EOD cycle from the ratio of the input firing rate to the EOD frequency, $p(t) = r(t)/f_\mathrm{EOD}$. Since $r(t)$ is bounded between 0 and f_EOD by Eq. 5, the resulting per-cycle firing probabilities $p(t)$ are bounded between 0 and 1. The firing probability $p(t)$ is then compared with a random number η chosen from a uniform distribution between 0 and 1 in order to determine whether or not to generate a spike event on each EOD cycle:

$$s(t) = \begin{cases} 0 & \eta > p(t) \\ 1 & \eta \le p(t) \end{cases} \tag{6}$$

The output spikes are initially generated at times corresponding to integral multiples of the EOD period. A small amount of time jitter is then added to simulate the degree of phase locking observed in the data. The time jitter for each spike is drawn from a normal distribution of random numbers with a zero mean and a standard deviation equal to 8% of the EOD period, as determined from an analysis of the widths of individual peaks in the experimental ISI histograms (Fig. 1B–D). An absolute refractory period equal to one EOD cycle is implemented, based on the observation that the first peak in the experimental ISI histograms is asymmetric and typically contains no intervals less than one full EOD period.

In an extended version of the spike-generating element, the firing regularity can be controlled with an additional parameter m. For $m > 1$, the extended model implements m independent random subprocesses each with an event rate equal to the spike rate $r(t)$. Each subprocess is simulated as described above using an update time step equal to the EOD period. Output spikes are generated at the time of occurrence of every m^th subprocess event. All other aspects of the model are as described above. Figure 10 shows representative baseline ISI distributions generated by the extended model for different values of m. A value of $m = 1$ produces an irregular firing pattern with an ISI distribution similar to that in Fig. 1B. A value of $m = 8$ produces a more regular firing pattern with an ISI distribution similar to that shown in Fig. 1C.

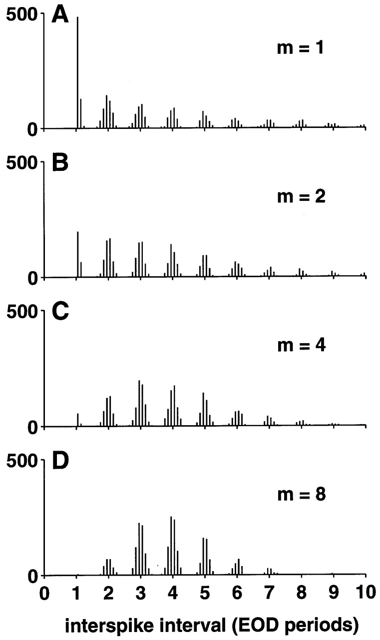

Fig. 10A–D Baseline interspike interval distributions produced by the stochastic spike-generating element in our model. **A–D** Distributions of increasing spike regularity with m = 1,2,4, and 8, respectively. All four ISI distributions have a mean of four EOD periods

Comparisons between experimental and simulated data sets

Figure 11 shows a representative comparison between experimental and computer simulated P unit response data. The simulated data set was generated using the computational model shown in Fig. 9 with a total of seven model parameters determined from fits to the experimental data: three gain terms $G_\mathrm{a-c}$ and two time-constants $\tau_\mathrm{a-b}$ in Eq. 1, the EOD frequency f_EOD in Eq. 5, and the parameter m controlling spike regularity. Once the parameters of the afferent model had been determined, computer simulations were carried out using a stimulus paradigm that was identical to that used in our experimental studies; thus, simulated data sets and experimental data sets could be analyzed using the same data analysis programs. As shown in Fig. 11, the model does an excellent job of reproducing the key features of the experimental data. Note that the simulated step response data (Fig. 11B2) exhibits slightly more spike rate variability than the actual data (Fig. 11B1). This is due to the fact that our spike generation model is based on first-order ISI statistics and does not include higher-order correlations. The vari-

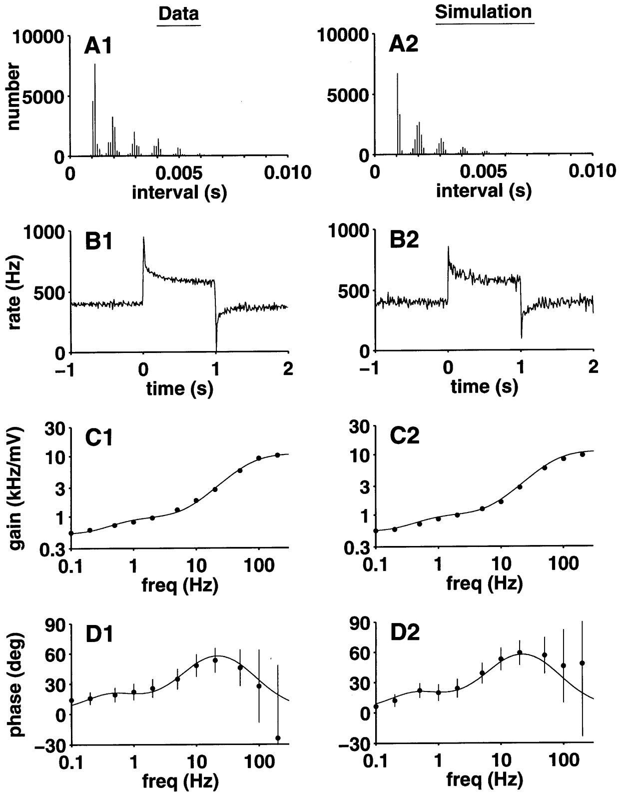

Fig. 11A–D Comparison of experimental (**A1–D1**) and simulated (**A2–D2**) data sets. **A** Baseline interspike interval distribution. **B** Response to an AM step stimulus (1 s duration, −10 dB amplitude). **C** Normalized gain versus AM frequency. **D** Phase versus AM frequency

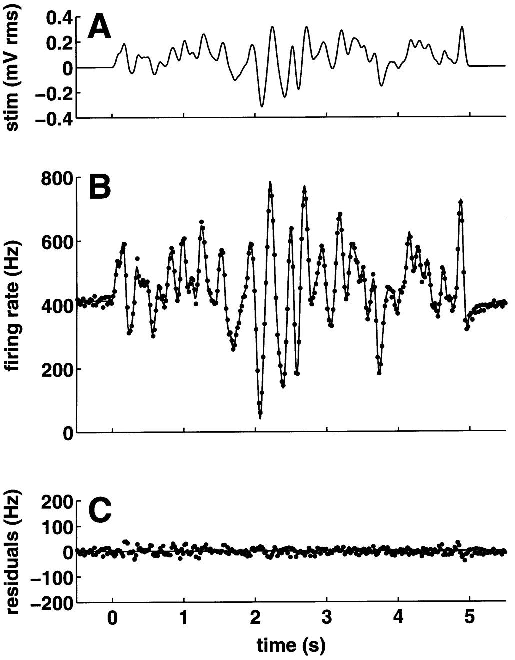

Fig. 12 Comparison of experimental and model responses to a complex AM stimulus. **A** AM stimulus envelope generated by passing Gaussian noise through a low-pass filter with a cutoff frequency of 5 Hz. **B** Predicted (*solid line*) versus measured (*data points*) change in afferent firing rate. **C** Residual error between predicted and measured response

ability in the high-frequency phase characteristics, apparent in both the experimental (Fig. 11D1) and simulated (Fig. 11D2) data sets, is associated with the overall variability in the response latency of the system.

The good agreement between experimental and simulated data sets in Fig. 11 is not too surprising, since the simulation was evaluated under the same conditions that were initially used to determine the model parameters. A more demanding test of the model involves comparing experimental and simulated data sets in response to a novel stimulus. To make this comparison, we constructed a complex AM stimulus waveform by passing Gaussian noise through a fourth-order Butterworth filter with a cutoff frequency of 5 Hz. The cutoff was chosen to emphasize AM frequency components that are probably of most relevance to prey detection using the active electric sense (see Discussion). This computer generated noise signal (Fig. 12A) was then used as the AM stimulus for obtaining both experimental and simulated afferent responses. Figure 12B shows a comparison between the experimentally measured change in afferent firing rate (data points) averaged over 20 presentations of the AM stimulus and the predictions of the simulation model (continuous solid curve). The excellent agreement between experimental data and the model prediction can be better appreciated by looking at the residuals as shown in Fig. 12C. Note that the degree of scatter in the residuals during the stimulation ($0 \le t \le 5$) is comparable to the scatter during the prestimulus interval ($t < 0$) when the firing rate is constant, indicating that the residuals are consistent with variance inherent in the experimental data points. Thus, the model is capable of accurately predicting responses to complex AM waveforms, such as those that might be encountered during natural electrolocation behaviors.

Discussion

New insights into P unit response dynamics

Our experimental results are in general agreement with previous studies by other investigators (Hagiwara et al. 1965; Scheich et al. 1973; Hopkins 1976; Shumway and Maler 1989), but our analysis provides some additional useful insights into the key features of P unit response dynamics. One important finding concerns the significance of the fast time-constant τ_a (Eq. 1), which we find to be approximately 2.5 ms (see Fig. 5B). As discussed in the Introduction, earlier studies have reported much longer time-constants, in the range of a few tenths of a second to several seconds. In this study, we find that our model must contain a fast time-constant with a value in the range of a few milliseconds in order to fit the high-frequency AM response characteristics. As shown in Fig. 4A, this fast time-constant dominates the AM frequency response characteristics for frequencies higher than about 20 Hz. This important component of P unit response dynamics had been missed in previous studies using AM step stimuli because the data were typically analyzed using bin widths that were too large to observe the rapid adaptation in the first few milliseconds of the response. Our recent study of P unit responses to AM step stimuli in *A. leptorhynchus* has verified that such fast adaptation components are indeed present in the step response data (Xu et al. 1996).

Although it was missed in earlier AM step response studies, the fast component of P unit response dynamics was implicit in the sinusoidal AM frequency response data presented by Bastian (1981), but he did not explicitly interpret the data in this way. Bastian's data showed that the gain of P units in *Apteronotus albifrons* is monotonically increasing up to AM frequencies of at least 64 Hz followed by a rolloff at higher frequencies (Bastian 1981). A high-pass filter with a corner frequency near 64 Hz should have a corresponding time-constant in the range of 2.5 ms ($1/2\pi f$), in good agreement with the value of τ_a obtained in this study.

Whereas Bastian observed a significant rolloff in gain for AM frequencies above 64 Hz in *A. albifrons*, we found that the gain in *A. leptorhynchus* continues to increase up to 100 Hz and then flattens out, but does not roll off significantly (see Fig. 3). This may be due to a species difference, or perhaps due to a difference in data analysis techniques. Based on the observed high-frequency rolloff, Bastian suggested that P units might be tuned to optimally detect AM modulations near 64 Hz. Since we do not observe a significant high-frequency rolloff in our data our interpretation is somewhat different. Our results suggest that P units in *A. leptorhynchus* are not tuned to a particular AM frequency, but rather that high-frequency components of the input signal are simply weighted more heavily than low-frequency components.

The increased weighting of high-frequency components may possibly arise from a need to maintain sensitivity across a broad range of AM frequencies when faced with an input amplitude spectrum that is likely to be dominated by low-frequency components. Although no quantitative experimental data on the frequency components of natural electrosensory scenes exists, we can gain some insight by making comparisons with the statistical properties of natural visual scenes, where the amplitude spectrum is known to vary approximately inversely with spatial frequency (i.e., a $1/f$ amplitude spectrum) (Field 1987; Ruderman and Bialek 1994). Electrosensory images are likely to be even more dominated by low frequencies than visual images due to the lack of a peripheral focusing mechanism (such as the lens of the eye) which results in electrosensory images that are increasingly blurred with increasing object distance (Rasnow 1996). If the electrosensory system is to maintain sensitivity to subtle high-frequency components of natural images while preventing the afferents from being driven into rectification or saturation by the more intense low-frequency components, then the primary afferents need to have intrinsic response dynamics that emphasize the high-frequency end of the input spectrum.

Afferent sensitivity

We measured the mean transverse gain of P-type afferents at 1 Hz to be 626 ± 328 spikes $\mathrm{s}^{-1}\mathrm{mV}^{-1}$ (Fig. 7). In *Apteronotus*, tuberous electroreceptor organs on the trunk tend to be clustered along the dorsal and ventral surfaces with a density of about 2–3 per mm^2, compared with about 1 per mm^2 along the midline (Carr et al. 1982). Thus, the transverse stimulus geometry used in this study, which is optimally oriented for units along the midline, was not optimal for most of the units in the sample. If we model the density distribution $\rho(\theta)$ of electroreceptor organs around the trunk as $\rho(\theta) = 2 - \cos(\theta)$, where θ values of $+90$, 0, and -90 correspond to dorsal, midline, and ventral positions respectively, and model the transverse gain as proportional to $\cos(\theta)$, we estimate that the mean response attenuation for a transverse stimulus relative to an optimally oriented stimulus, averaged over the population of units, is 0.57. Thus, we estimate that the average gain of P units for an optimally oriented 1-Hz stimulus would be about 1100 spikes $\mathrm{s}^{-1}\mathrm{mV}^{-1}$.

Sensitivity to weak AM stimuli

Behavioral and physiological thresholds in *Apteronotus* have been estimated to be in the region of 0.1 μV RMS (Rasnow 1996). To estimate afferent responses to such weak stimuli requires extrapolating from stimulus-response data obtained using stronger stimuli. As illustrated in Fig. 8B, the results of the extrapolation depend critically on assumptions about response linearity. One convenient benchmark for describing afferent sensitivity to weak stimuli is to quote the stimulus intensity that causes a 1 spike s^{-1} change in afferent firing rate (Bastian 1981). Assuming a power law form $y = Ax^{\mathrm{B}}$ and solving for the stimulus strength x when $y = 1$ spike s^{-1} yields $x = A^{-1/\mathrm{B}}$, where A is the gain and B is the power law exponent. Using a gain value of $A = 1100$ spikes $\mathrm{s}^{-1}\mathrm{mV}^{-1}$ from the above analysis and a linear extrapolation ($B = 1$) (cf. solid line in Fig. 8B), we predict that a 1 spike s^{-1} change can be elicited by a 0.9-μV RMS stimulus. If we use the same value of A, but extrapolate using our best-fit value of $B = 0.9$ (cf. dashed line in Fig. 8B), we predict that 0.42 μV RMS is sufficient to elicit a 1 spike s^{-1} change, which is a factor of 2 smaller than obtained from the linear extrapolation. In general, power law extrapolations with $B < 1$ predict greater afferent sensitivity at low stimulus strengths than a linear extrapolation with $B = 1$.

In a study of P units in *A. albifrons,* Bastian (1981) reported a best-fit power law exponent of $B = 0.77$ and estimated that a 1 spike s^{-1} change in afferent firing corresponded to a field strength of 0.9 $\mu\mathrm{V\ cm}^{-1}$ peak-to-peak measured in the water outside the fish. Using estimates of skin and water resistivity, Rasnow (1996) computed that this field strength corresponds to a 0.1 μV RMS change in transdermal potential. If Bastian had used a linear extrapolation ($B = 1$) rather than a power law extrapolation with $B = 0.77$, his prediction would have been about 0.8 μV RMS change in transdermal voltage, which is in good agreement with our linear extrapolation of 0.9 μV RMS. Based on the uncertainties in the best-fit power law exponent, we conclude that existing data is consistent with a 1 spike s^{-1} change in afferent firing rate corresponding to a change in transdermal potential somewhere in the range of 0.1–1.0 μV RMS. It should be noted that these numbers are for a 1-Hz AM stimulus. Afferents will be more sensitive to higher AM frequencies and less sensitive to lower AM frequencies, as summarized in Fig. 3.

Implications for detection of small prey

It is informative to compare these numbers with estimates of the transdermal potential modulations generated by natural electrolocation targets. We are currently carrying out infrared video recording experiments of prey capture in *A. albifrons* and *A. leptorhynchus* and have observed qualitatively similar behavior in these two species. In *A. albifrons* we have obtained preliminary quantitative data showing that *Daphnia magna* (2–3 mm diameter) can be detected in the absence of visual cues at a distance of about 2 cm when the fish is swimming at a typical search velocity of about 10 cm s^{-1} (MacIver et al. 1997). Based on the physics of electric image formation for spherical objects, the peak transdermal potential modulation for a 3 mm diameter sphere, 2 cm from the midline, is about a 0.2 μV RMS increase for a perfect conductor and a 0.1 μV RMS decrease for a perfect insulator (Rasnow 1996). While we do not have experimentally measured conductivity values for *Daphnia*, the preceding values set bounds on the magnitude of the voltage change. To determine how strongly P units would respond to a stimulus of this magnitude we also need to know the corresponding AM frequency spectrum. Again using results from Rasnow (1996), the full width at half maximum for the electric image cast by a 3-mm sphere at a distance of 2 cm from the electroreceptor array is estimated to be about 2 cm. The spatial frequency components of this image, computed from the Fourier transform, have a spectrum with a half-amplitude bandwidth of about 0.22 cycles cm^{-1}. When the image is moving with a velocity of 10 cm s^{-1} across the receptor array, this gives rise to a temporal frequency spectrum with a bandwidth of about 2.2 Hz. Thus, around the time of detection, the image cast by a *Daphnia* is estimated to have a peak magnitude of about 0.1 μV RMS and an AM frequency bandwidth of about 2.2 Hz. Using the afferent gain extrapolations for weak stimuli at 1 Hz described above, this corresponds to a change in afferent firing rate between 0.1 and 1.0 spikes s^{-1}. Such a small change could not be detected on an individual afferent fiber due to the intrinsic variability in afferent spike rate, but the electric image influences a significant number of afferent fibers; for a typical trunk receptor organ density of 1–2 mm^{-2}, there will be approximately 300–600 electroreceptor organs within the 2-cm-diameter region corresponding to the image full width at half maximum.

The above discussion is not intended to suggest that AM signals provide the only possible sensory cue for prey localization in the dark. Small prey can potentially generate phase shifts which could be detected by T-type tuberous receptor organs, low-frequency electrical signals which could be detected by ampullary receptors, and mechanical vibrations which could be detected by mechanosensory lateral line receptors.

Extensions to the model to accommodate longer time scales

The lowest frequency sinusoidal AM stimulus used in this study was 0.1 Hz which, if taken as the corner frequency of a first-order filter, would correspond to a time-constant of 1.6 s. Thus, the experimental data collected in this study cannot provide insights into components of P unit response dynamics that correspond to longer time scales. From our recent study of P unit responses to prolonged AM steps, we know that the firing rate of P units continues to adapt slowly for time periods up to several hundred seconds after the step onset, implying that the response dynamics includes slow components (Xu et al. 1996). Analysis of the AM step response data demonstrated that the time-course of sensory adaptation in P units could be accurately described by a functional form in which the change in afferent firing rate Δr decays logarithmically with time according to an equation of the form: $\Delta r = A/(B\ln(t) + 1)$. This form accurately describes the adaptation time-course of P-type afferents over five decades in time from milliseconds to hundreds of seconds using only two free parameters. Figure 13A compares the normalized adaptation time-course in response to an AM step stimulus predicted by the logarithmic decay function (dashed line) and the normalized step response predicted by the linear model of Eq. 2 (solid line), $\Delta r_{\mathrm{step}} = g_{\mathrm{a}}\mathrm{e}^{-t/\tau_{\mathrm{a}}} + g_{\mathrm{b}}\mathrm{e}^{-t/\tau_{\mathrm{b}}} + g_{\mathrm{c}}$, using the same parameters as in Fig. 3: $g_{\mathrm{a}} = 11.3$, $g_{\mathrm{b}} = 0.37$, $g_{\mathrm{c}} = 0.63$, $\tau_{\mathrm{a}} = 0.0029$ s, and $\tau_{\mathrm{b}} = 0.318$ s. In general the curves are similar, but the linear model of Eq. 2 predicts a lower firing rate for times between about 10 and 100 ms, and predicts a higher firing rate for times greater than 1 s. Since our experimental data using AM sinusoids do not provide insights into the response dynamics for time scales longer than about 1 s, we can use the logarithmic parameterization of the step response data from Xu et al. (1996) to adapt the linear model of Eq. 2 to give a better

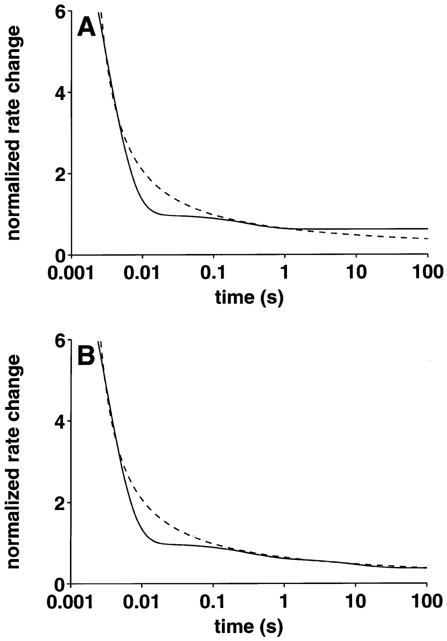

Fig. 13A, B Model predictions for the adaptation time-course of P-type afferents in response to a prolonged AM step stimulus shown on a logarithmic time scale. **A** Comparison of the logarithmic adaptation model (Xu et al. 1996): $\Delta r = A/(B\ln(t) + 1)$ with $A = 0.64$ and $B = 0.15$ (*dashed line*) and the *two*-time-constant model of Eq. 2 (*solid line*) using best-fit parameters from Fig. 3: $g_a = 11.3$, $g_b = 0.37$, $g_c = 0.63$, $\tau_a = 0.0029$ s, and $\tau_b = 0.32$ s. **B** Comparison of the same logarithmic adaptation model (*dashed*) shown in **A** and the *three*-time-constant model (*solid*) of Eq. 7; note the improved agreement for times greater than 1 s. Parameter values: $g_a = 11.3$, $g_b = 0.37$, $g_{slow} = 0.25$, $g'_c = 0.37$, $\tau_a = 0.0029$ s, $\tau_b = 0.32$ s, and $\tau_{slow} = 10.0$ s

approximation of the long time scale behavior by adding a third slower time-constant:

$$H_{norm}(s) = \frac{g_a s}{s + 1/\tau_a} + \frac{g_b s}{s + 1/\tau_b} + \frac{g_{slow} s}{s + 1/\tau_{slow}} + g'_c \qquad (7)$$

where $g_{a\text{–}b}$ and $\tau_{a\text{–}b}$ are the same as in Eq. 1, but the constant gain term g_c in Eq. 1 has been replaced by two terms: a high-pass filter term with gain g_{slow} and time-constant τ_{slow} and a new constant gain term g'_c. Figure 13B compares the logarithmic adaptation time-course (dashed line) with the modified form of the linear model in Eq. 2 with $g'_c = 0.6\,g_c$, $g_{slow} = 0.4\,g_c$, and $\tau_{slow} = 10\,\text{s}$. The modified model of Eq. 7 does a good job of describing the continued firing rate adaptation for times longer than 1 s.

From a practical point of view, the decision of whether to use the two-time-constant model of Eq. 2 or the three-time-constant model of Eq. 7 in a computer simulation study depends on whether the stimulus paradigm being simulated will involve prolonged AM steps or signals with slow (< 0.1 Hz) AM frequency components. For example, some of the classic gain control experiments (Bastian 1986b, c) and pyramidal cell adaptation studies (Bastian and Courtright 1991) in the electrosensory lateral line lobe were carried out using prolonged AM steps to mimic steady-state increases or decreases in the fish's EOD strength. Thus, the three-time-constant model of Eq. 7 would yield a more accurate description of P unit responses under these conditions than the model of Eq. 2.

Interpretation of model parameters

As shown in Xu et al. (1996), the time-course of sensory adaptation in P units could be accurately described by the logarithmic decay function $\Delta r = A/(B\ln(t) + 1)$ using just two free parameters, whereas fitting the adaptation time-course using a sum of exponentials $\Delta r(t) = A_1 e^{-t/\tau 1} + A_2 e^{-t/\tau 2} + \cdots + A_n e^{-t/\tau_n} + C$ required a total of nine free parameters (four time-constants, four corresponding amplitude parameters, and one constant term) to produce a fit with a χ^2 per DOF comparable to that obtained with the two-parameter logarithmic form. Given that the logarithmic form provides a more efficient description of the adaptation time-course than a multiexponential form, it is natural to ask why we chose to construct our transfer functions in this paper (Eqs. 1, 2, 7) from a sum of linear first-order high-pass filter terms that have exponential step responses, rather than using a non-linear differential equation with a logarithmic step response. The principal reason for this choice is associated with the observation that P units have nearly linear response characteristics, as determined from analysis of intensity response profiles (Fig. 8B) and tests of responses to sums of sinusoids with different AM frequencies. Linear response characteristics can be ensured by summing the contributions of multiple linear components, such as the first-order high-pass filters used in our model. This consideration of response linearity led us to the formulation used in this paper.

As described in Xu et al. (1996), P unit response dynamics appear to involve time scales ranging continuously from milliseconds to tens of seconds. This wide range of time scales is likely to arise from multiple spatially and temporally distributed relaxation processes covering a wide range of time-constants, as has been proposed as a basis for power law adaptation observed in other systems (Thorson and Biederman-Throson 1974). Thus, the time-constants τ_a, τ_b, and τ_{slow} reported in this study should not be assumed to correspond to discrete underlying biophysical processes, but should be thought of as terms in a series expansion in which first-order high-pass filter elements are used as a basis set for approximating the higher-order distributed dynamics of P-type afferents.

Scope and limitations of the model

The model of P-type afferent response dynamics described in this paper was designed to serve as part of an integrated computational model of electrolocation, with a scope that extends from peripheral electric image formation (Rasnow 1996) to adaptive filtering in the electrosensory lateral line lobe (Bastian 1995). In this context, the two principal design goals for the afferent model were that it accurately describe the sensory encoding process over the range of AM frequencies that is relevant for electrolocation behaviors, and that the model be computationally efficient, so that it would be possible to simulate the responses of the entire population of several thousand P-type afferents during a typical behavioral sequence lasting several seconds. These design goals led to the development of an empirical model of afferent response dynamics in which the essential dynamic characteristics are captured using a relatively small number of experimentally constrained parameters, rather than to the development of a biophysically detailed model of the underlying mechanisms. A more biophysically based model, such as that developed recently by Kashimori et al. (1996), would have involved a significantly larger number of differential equations for updating dynamic state variables, and a correspondingly larger number of model parameter values, many of which would be related to cellular and synaptic processes for which we do not have good experimental constraints. Whereas the Kashimori model is concerned primarily with elucidating microscopic mechanisms at the single receptor cell level, our model is focused on accurately characterizing the macroscopic dynamic properties of the afferent system as a whole, and thus we see these efforts as complementary. As a result of the tradeoffs inherent in reducing the amount of biophysical detail to increase computational efficiency, the model presented in this paper can only be used to simulate P unit responses to those stimuli for which it was developed, namely amplitude modulations of a fixed-frequency carrier signal corresponding to the fish's own EOD. As currently formulated, the model is not appropriate for accurately predicting P unit responses to signals arising from interactions with other weakly electric fish, such as jamming interactions or electrocommunication signals, or responses to externally imposed electrical stimuli at frequencies other than the fish's own EOD frequency.

Acknowledgements This research was supported by a grant from the National Institute of Mental Health (R29 MH49242).

References

Bastian J (1974) Electrosensory input to the corpus cerebelli of the high frequency electric fish *Eigenmannia virescens*. J Comp Physiol A 90: 1–24

Bastian J (1981) Electrolocation I. How the electroreceptors of *Apteronotus albifrons* code for moving objects and other electrical stimuli. J Comp Physiol A 144: 465–479

Bastian J (1986a) Electrolocation: Behavior, anatomy, and physiology. In: Bullock TH, Heiligenberg W (eds) Electroreception. Wiley, New York, pp 577–612

Bastian J (1986b) Gain control in the electrosensory system mediated by descending inputs to the electrosensory lateral line lobe. J Neurosci 6: 553–562

Bastian J (1986c) Gain control in the electrosensory system: a role for the descending projections to the electrosensory lateral line lobe. J Comp Physiol A 158: 505–516

Bastian J (1995) Electrolocation. In: Arbib MA (ed) The handbook of brain theory and neural networks. MIT Press, Cambridge, Mass, pp 352–356

Bastian J, Courtright J (1991) Morphological correlates of pyramidal cell adaptation rate in the electrosensory lateral line lobe of weakly electric fish. J Comp Physiol A 168: 393–407

Carr CE, Maler L, Sas E (1982) Peripheral organization and central projections of the electrosensory nerves in gymnotiform fish. J Comp Neurol 211: 139–153

Field DJ (1987) Relations between the statistics of natural images and the response properties of cortical cells. J Opt Soc Am A 4: 2379–2394

Hagiwara S, Szabo T, Enger PS (1965) Electroreceptor mechanisms in a high-frequency weakly electric fish, *Sternarchus albifrons*. J Neurophysiol 28: 784–799

Heiligenberg W, Dye J (1982) Labelling of electroreceptive afferents in gymnotid fish by intracellular injection of HRP: the mystery of multiple maps. J Comp Physiol A 148: 287–296

Heiligenberg W, Partridge BL (1981) How electroreceptors encode JAR-eliciting stimulus regimes: reading trajectories in a phase-amplitude plane. J Comp Physiol A 142: 295–308

Hopkins CD (1976) Stimulus filtering and electroreception: tuberous electroreceptors in three species of gymnotoid fish. J Comp Physiol A 111: 171–207

Kashimori Y, Goto M, Kambara T (1996) Model of P- and T-electroreceptors of weakly electric fish. Biophys J 70: 2513–2526

MacIver MA, Lin JL, Nelson ME (1997) Estimation of signal characteristics during electrolocation from video analysis of prey capture behavior in weakly electric fish. In: Bower J (ed) Computational Neuroscience '96. Plenum Boston, (in press)

Rasnow B (1996) The effects of simple objects on the electric field of *Apteronotus*. J Comp Physiol A 178: 397–411

Ruderman DL, Bialek W (1994) Statistics of natural images: scaling in the woods. Phys Rev Lett 73: 814–817

Scheich H, Bullock TH, Hamstra RHJ (1973) Coding properties of two classes of afferent nerve fibers: high frequency electroreceptors in the electric fish *Eigenmannia*. J Neurophysiol 36: 39–60

Shumway CA, Maler LM (1989) GABAergic inhibition shapes temporal and spatial response properties of pyramidal cells in the electrosensory lateral line lobe of gymnotiform fish. J Comp Physiol A 164: 391–407

Thorson J, Biederman-Thorson M (1974) Distributed relaxation processes in sensory adaptation. Science 183: 161–172

Wessel R, Koch C, Gabbani F (1996) Coding of time-varying electric field amplitude modulations in a wave-type electric fish. J Neurophysiol 75: 2280–2293

Xu Z, Payne JR, Nelson ME (1996) Logarithmic time-course of sensory adaptation in electrosensory afferent nerve fibers in a weakly electric fish. J Neurophysiol 76: 2020–2032

Yager DD, Hopkins CD (1993) Directional characteristics of tuberous electroreceptors in the weakly electric fish, *Hypopomus* (Gymnotiformes). J Comp Physiol A 173: 401–414

Zakon HH (1986) The electroreceptive periphery. In: Bullock TH, Heiligenberg W (eds) Electroreception. Wiley, New York, pp 103–156